Supporting Information for

$NiFe_2O_4$ Nanoparticles/NiFe Layered Double-Hydroxide Nanosheet Heterostructure Array for Efficient Overall Water Splitting at Large Current Densities

Zhengcui Wu,* Zexian Zou, Jiansong Huang, and Feng Gao*

Anhui Laboratory of Molecule-Based Materials (State Key Laboratory Cultivation Base), The Key Laboratory of Functional Molecular Solids, Ministry of Education, College of Chemistry and Materials Science, Anhui Normal University, Wuhu 241002, P. R. China.

*Corresponding author. E-mail: zhengcui@mail.ahnu.edu.cn; fgao@mail.ahnu.edu.cn.

Tel.: +86 553 3869302; Fax: +86 553 3869302.

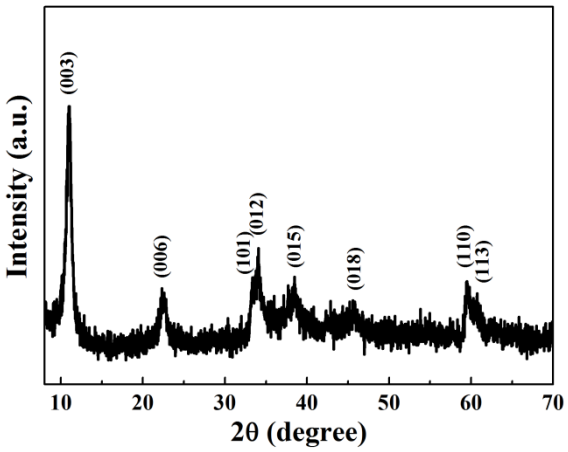

Figure S1. The XRD pattern of the precursor with Ni/Fe ratio of 1:2 in 5 mL of deionized water and 30 mL of methanol, showing it was the NiFe LDH phase.

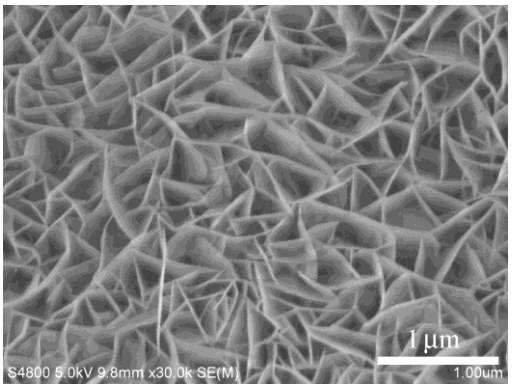

Figure S2. The SEM image of the NiFe LDH nanosheet array.

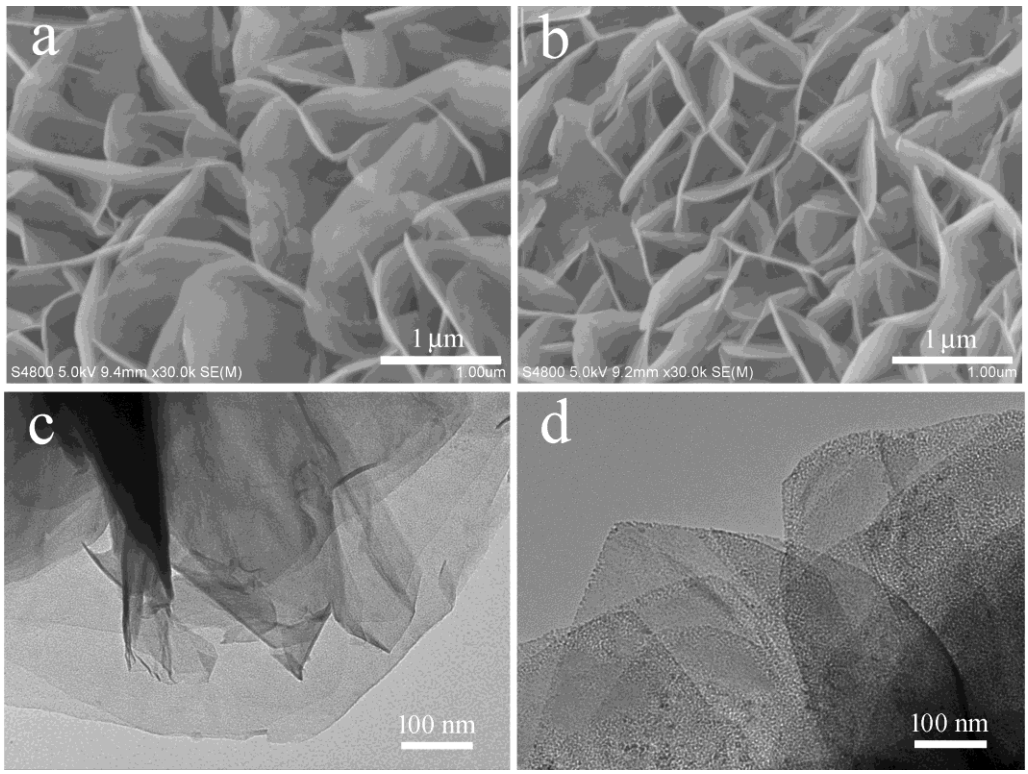

Figure S3. (a, b) The SEM images of the $NiFe_2O_4$ precursor nanosheet array and the $NiFe_2O_4$ nanosheet array, respectively. (c, d) The TEM images of $NiFe_2O_4$ precursor nanosheets and $NiFe_2O_4$ nanosheets, respectively.

The product of $NiFe_2O_4$ maintained the nanosheet array structure of its precursor as shown in Figure S3a,b. The TEM image of the $NiFe_2O_4$ precursor showed it was flexible nanosheets (Figure S3c), while that of $NiFe_2O_4$ presented many tiny mesoporosities on the nanosheets (Figure S3d), due to the release of water molecules by calcination. The similar nanosheets morphology conservation was also observed in some transition metal oxides obtained by calcining the corresponding precursors.[1, 2]

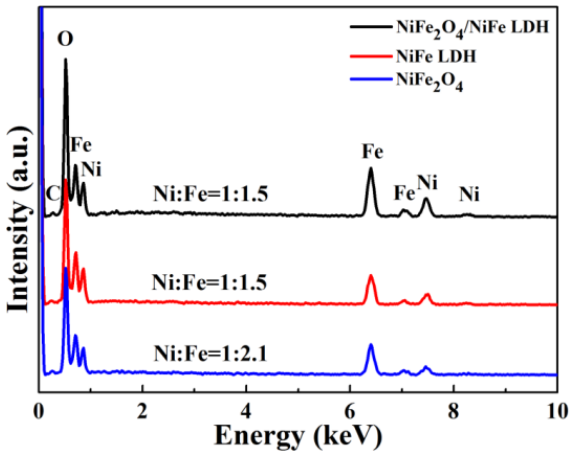

Figure S4. The EDX results of $NiFe_2O_4$/NiFe LDH, NiFe LDH, and $NiFe_2O_4$.

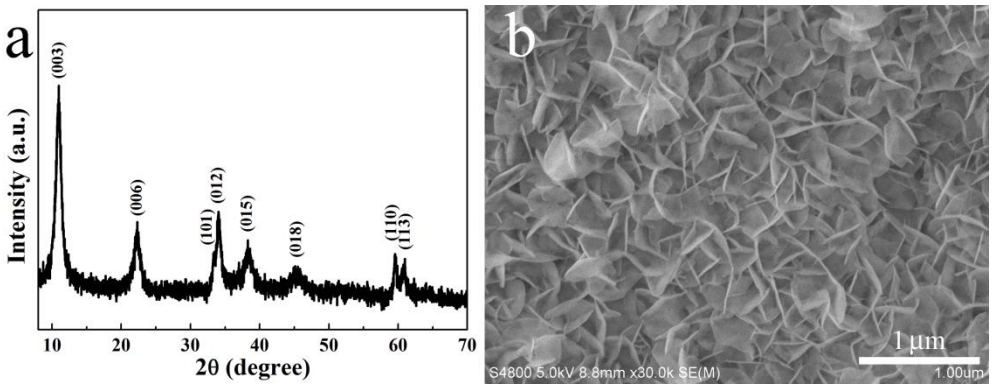

Figure S5. The XRD pattern (a) and SEM image (b) of the product with $FeCl_3 \cdot 6H_2O$ instead of $FeCl_2 \cdot 6H_2O$.

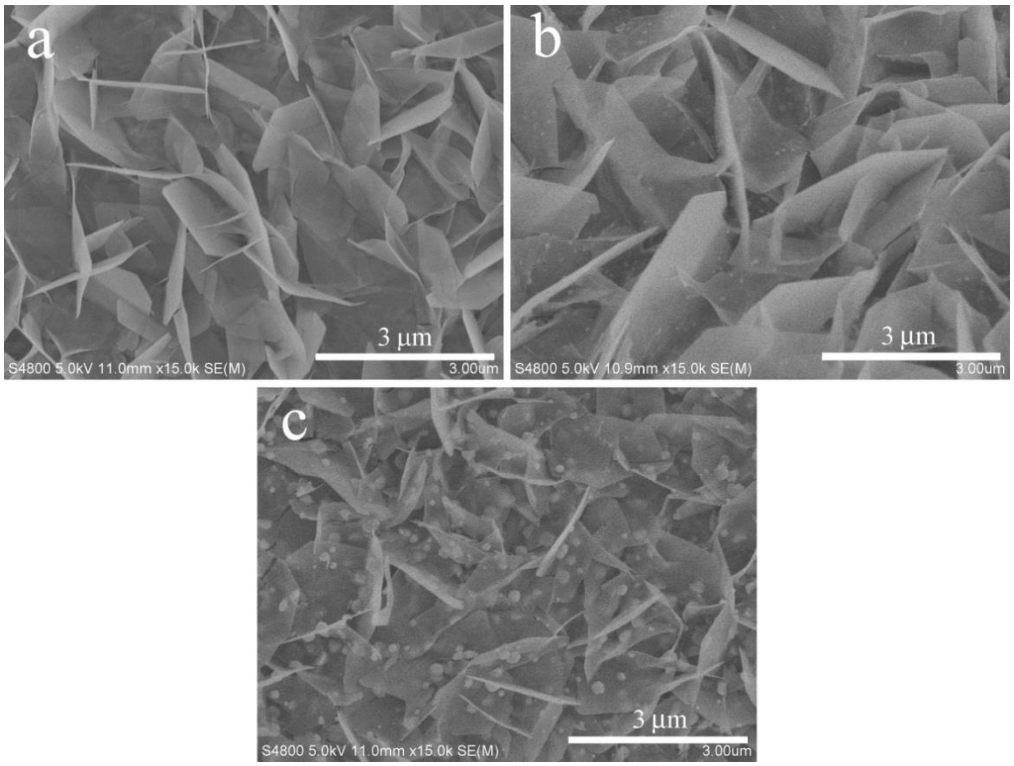

Figure S6. Time resolved experiments of $NiFe_2O_4$/NiFe LDH. (a) 30 min, (b) 60 min, and (c) 90 min.

Table S1. The comparison of OER activity of $NiFe_2O_4$/NiFe LDH with some representative NiFe bimetallic OER catalysts.

Catalyst	Electrolyte	η(mV) @j (mA cm^{-2})	Tafel Slope (mV dec^{-1})	Electrode	Reference
$Ni_3Fe(OH)_9$ nanosheets	1 M KOH 10 M KOH	270@80 240@500	28	Ni foam	[3]
NiFe LDH	1 M NaOH	210@10, 240@50, 260@100	31	Ni foam	[4]
NiFe-OH@Ni_3S_2 nanosheets	1 M KOH	165@10, 240@100	93	Ni foam	[5]
$NiFeO_x$ film	1 M KOH	260@100	28	Ni foam	[6]
Single-layer NiFe-LDH	1 M KOH	~300@10	40	Ni foam	[7]
NiFe-LDH nanoplatelet	1 M KOH	224@10	52.8	Ni foam	[8]
NiFe-rGO LDH	1 M KOH	206@10	39	Ni foam	[9]
$Ni_{0.71}Fe_{0.29}(OH)_x$	0.1 M KOH	296@10	58	graphite	[10]
NiFe-LDH/G	0.1 M KOH	325@10	44	Ni foam	[11]
NiFe hydroxide nanosheets	1 M KOH	220@10	40.7	Glassy carbon	[12]
NiFe LDH/C	0.1 M KOH	350@10	59	Ni foam	[13]
[Ni, Fe]O nanoparticles	0.1 M KOH	300-470@10	36-48	ITO	[14]
$FeNiO_x$ nanoparticles	1 M KOH	315@50	38	Glassy carbon	[15]
$Ni_{1-x}Fe_xO_y$ nanorods	1 M KOH	302@10	42	Glassy carbon	[16]
$NiFe_2O_4$/NiFe LDH	1 M KOH	213@100, 242@500, 265@1000	28.2	Ni foam	this work

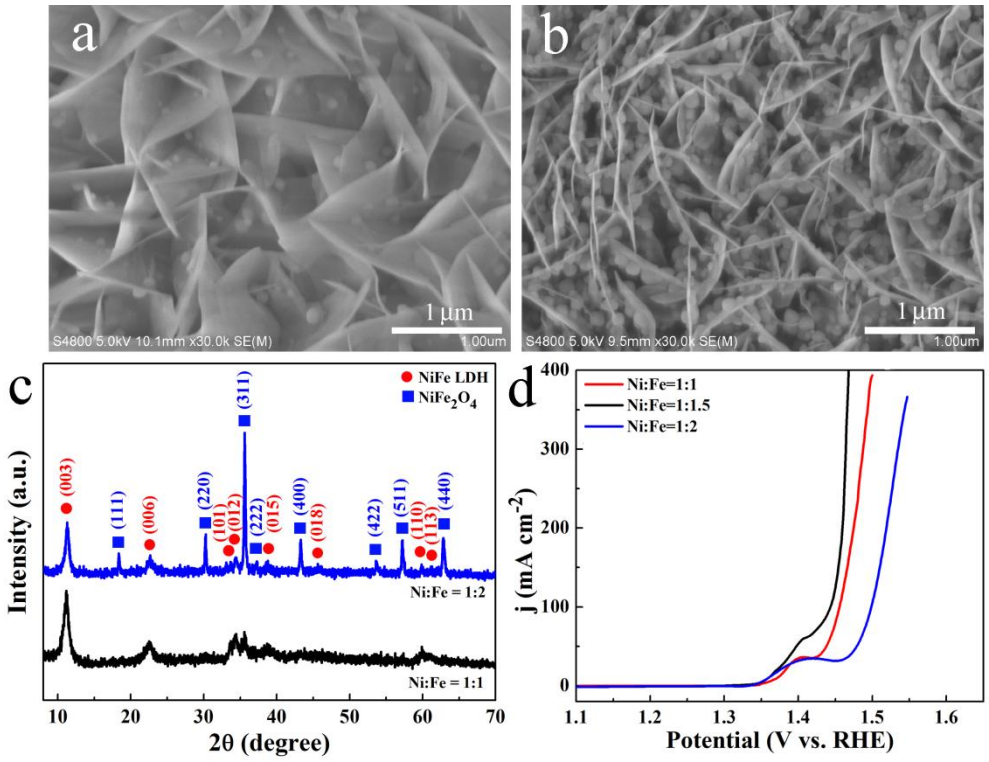

Figure S7. (a, b) The SEM images of the $NiFe_2O_4$/NiFe LDH products with Ni/Fe ratio of 1:1 and 1:2, respectively. (c) The XRD patterns of the $NiFe_2O_4$/NiFe LDH products with Ni/Fe ratio of 1:1 and 1:2. (d) The OER polarization curves of the $NiFe_2O_4$/NiFe LDH products with different ratio of Ni and Fe.

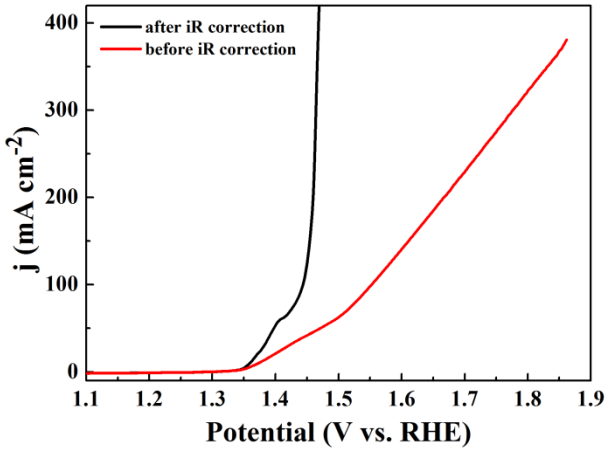

Figure S8. The OER LSV curves of $NiFe_2O_4$/NiFe-LDH electrode with and without iR-correction.

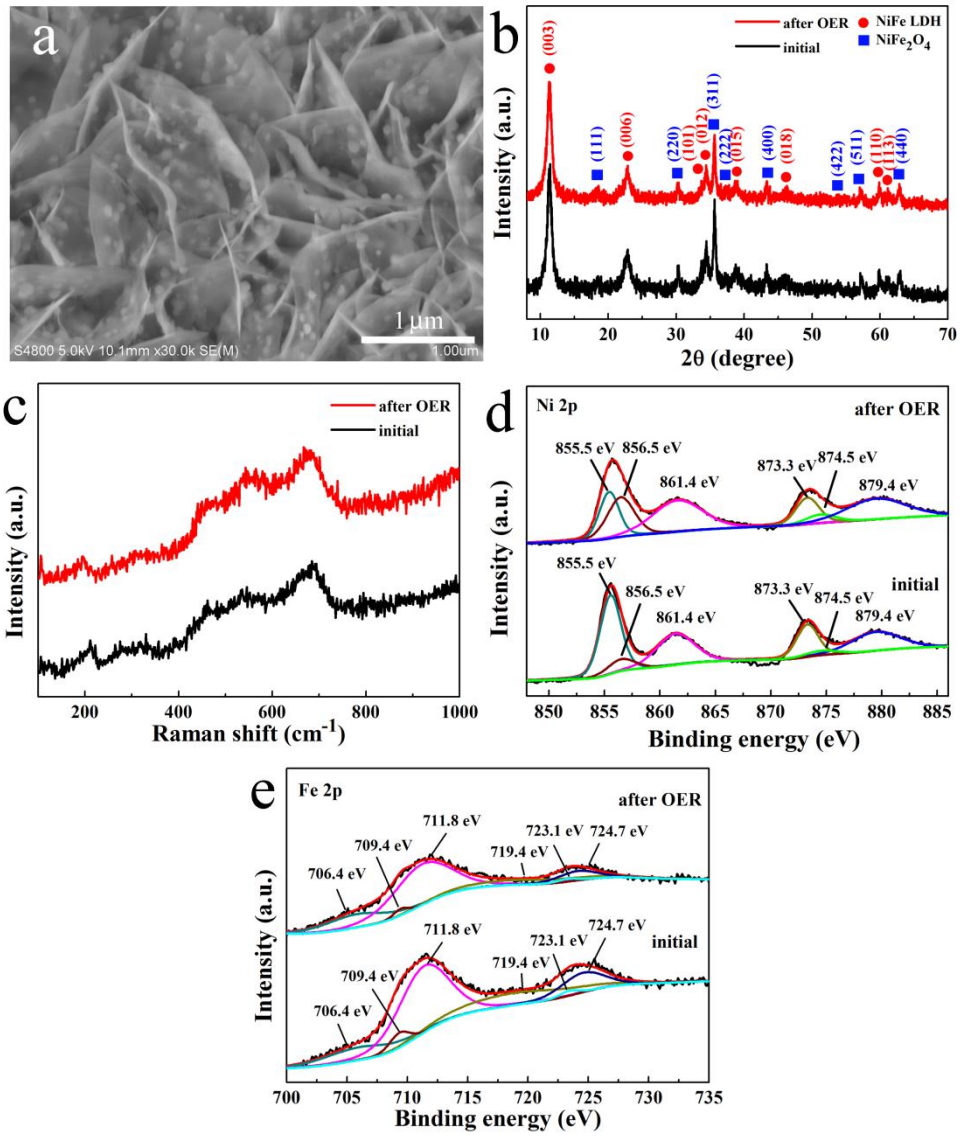

Figure S9. The SEM image (a), the XRD pattern (b), the Raman spectrum (c), the XPS spectra of Ni 2p (d) and Fe 2p (e) of $NiFe_2O_4$/NiFe LDH after 20 h OER chronopotentiometry test at overpotential of 202 mV.

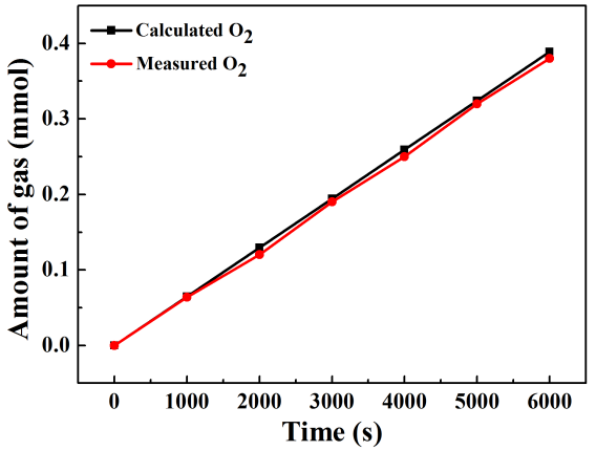

Figure S10. The electrocatalytic efficiency of $NiFe_2O_4$/NiFe-LDH for OER at 100 mA cm^{-2}.

Table S2. The comparison of HER activity of $NiFe_2O_4$/NiFe LDH with some representative NiFe bimetallic HER catalysts.

Catalyst	Electrolyte	η(mV) @j (mA cm^{-2})	Tafel Slope ($mV\ dec^{-1}$)	Electrode	Reference
NiFeP	1 M KOH	255@10	83	NiFe foil	[17]
NiFeS	1 M KOH	180@10	53	Ni foam	[18]
Fe-doped NiS_2 nanosheets	0.5 M H_2SO_4	121@10	37	Glassy carbon	[19]
Fe-doped Ni_2P nanosheets	1 M KOH	106@10	89.7	Ni foam	[20]
NiFe hydroxide nanosheets	1 M KOH	189@10	87.2	Glassy carbon	[12]
$FeNiP_x$ nanosheets	1 M KOH	161@100	80	Ni foam	[21]
Yolk-shell Ni_3Fe/Ni_3FeN	1 M KOH	166@10	127	Ni foam	[22]
NiFe-NGT-800	0.5 M H_2SO_4	150@18	63.4	Glassy carbon	[23]
$NiFe_2O_4$/NiFe LDH	1 M KOH	101@10, 297@500, 314@750	67.1	Ni foam	this work

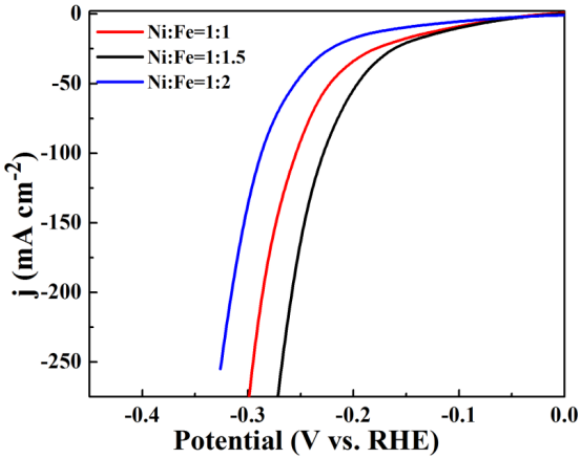

Figure S11. The HER polarization curves of the $NiFe_2O_4$/NiFe LDH products with different ratio of Ni and Fe.

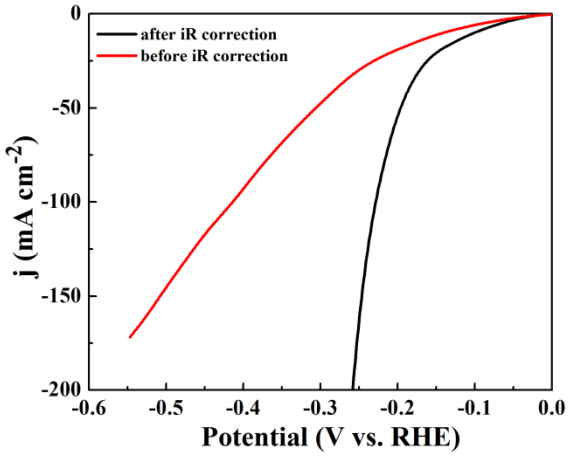

Figure S12. The HER LSV curves of $NiFe_2O_4$/NiFe-LDH electrode with and without iR-correction.

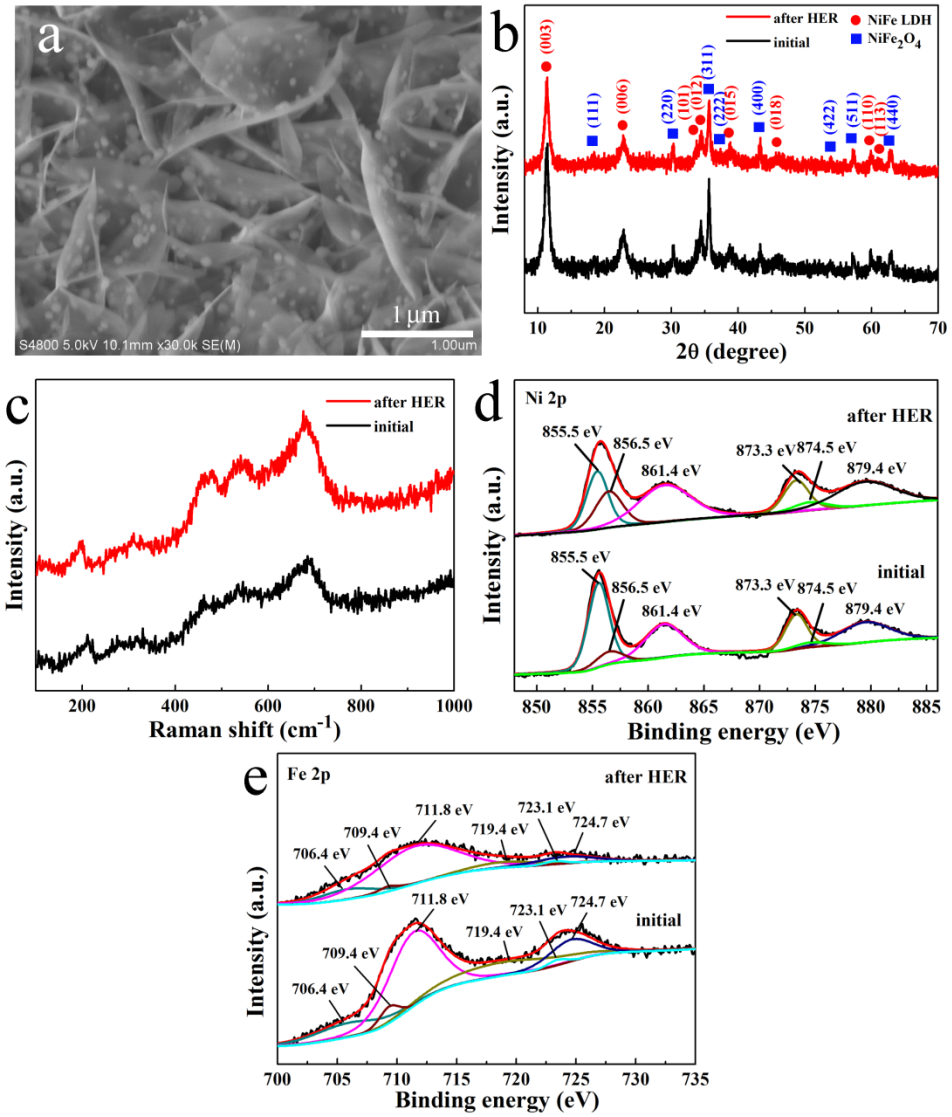

Figure S13. The SEM image (a), the XRD pattern (b), the Raman spectrum (c), the XPS spectra of Ni 2p (d) and Fe 2p (e) of $NiFe_2O_4$/NiFe LDH after 20 h HER chronopotentiometry test at overpotential of 150 mV.

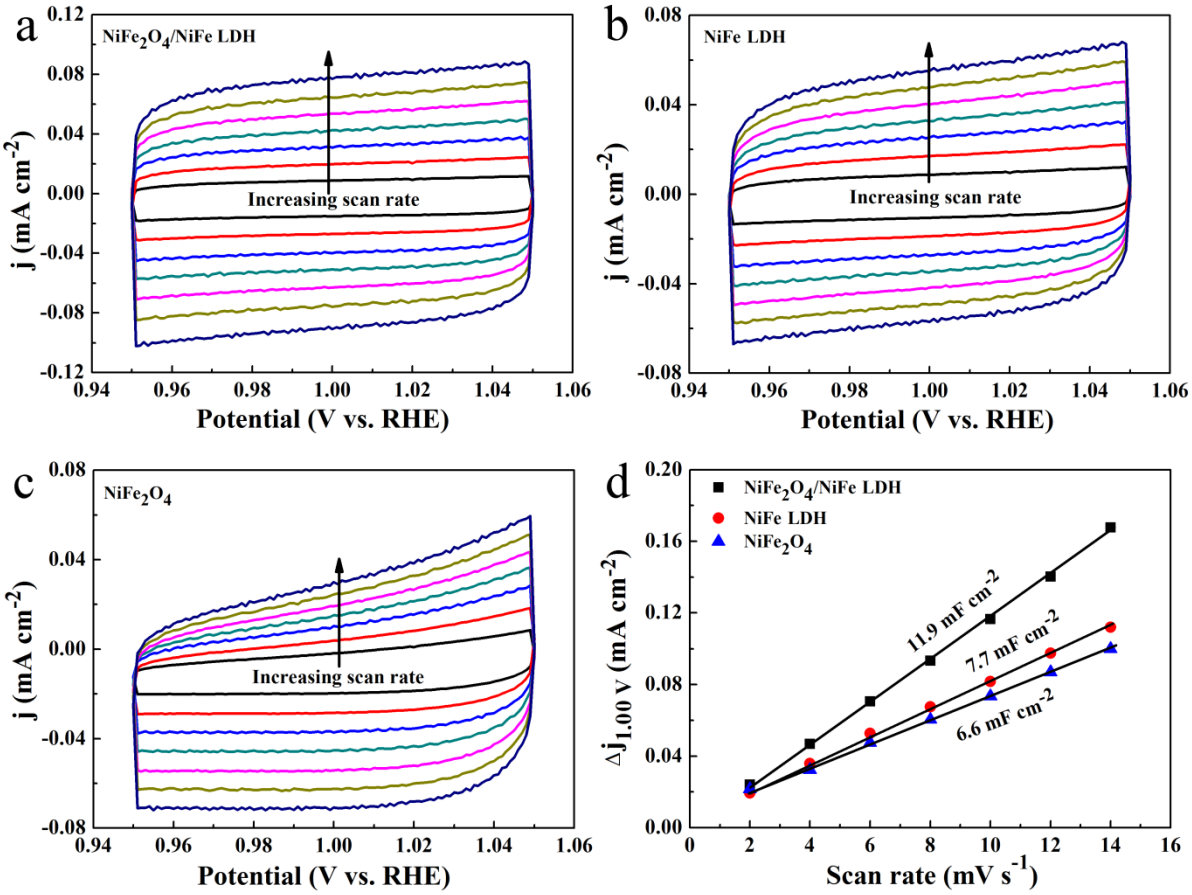

Figure S14. The cyclic voltammograms of $NiFe_2O_4$/NiFe LDH (a), NiFe LDH (b), and $NiFe_2O_4$ (c) at different scan rates of 2, 4, 6, 8, 10, 12, and 14 mV s^{-1}. (d) The capacitive currents at 1.00 V versus RHE with different scan rates.

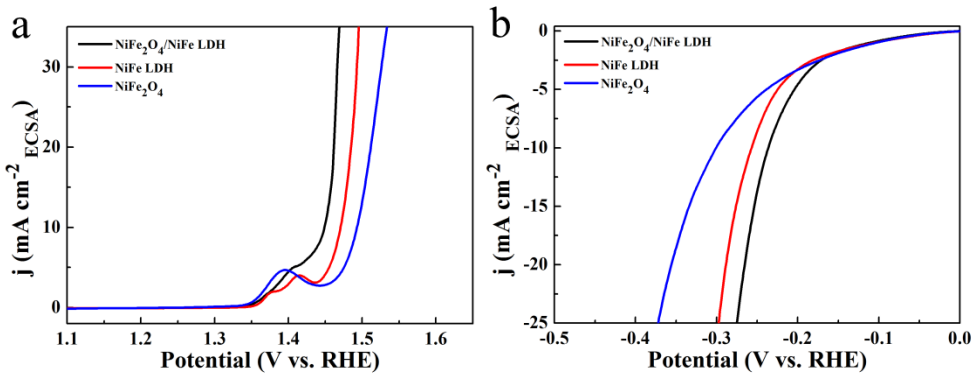

Figure S15. The ECSA-normalized LSV curves of $NiFe_2O_4$/NiFe LDH, NiFe-LDH, and $NiFe_2O_4$ for OER (a) and HER (b).

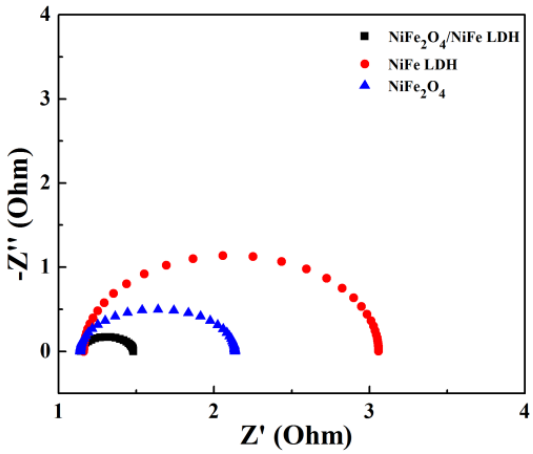

Figure S16. The fitting results of the semicircles of EIS of $NiFe_2O_4$/NiFe LDH, NiFe-LDH, and $NiFe_2O_4$.

Table S3. The comparison of the two-electrode overall water-splitting performance of $NiFe_2O_4$/NiFe LDH with some representative NiFe bimetallic electrocatalysts.

Catalyst	Electrolyte	Potential (V) @j (mA cm^{-2})	Electrode	Reference
NiFe hydroxide nanosheets	1 M KOH	1.67@10	Glassy carbon	[12]
Fe-doped Ni_2P nanosheet arrays	1 M KOH	1.61@10	Ni foam	[20]
$FeNiP_x$ nanosheets	1 M KOH	1.53@10, 1.74@50	Ni foam	[21]
Yolk-shell Ni_3Fe/Ni_3FeN	1 M KOH	1.62@10	Ni foam	[22]
NiFe@NC	1 M KOH	1.81@10	Glassy carbon	[24]
NiFe LDH-NS@DG10	1 M KOH	1.5@20	Ni foam	[25]
$Ni_{0.9}Fe_{0.1}$/NC	1 M KOH	1.58@10	Ni foam	[26]
$NiFe_2O_4$/NiFe LDH	1 M KOH	1.535@10, 1.932@500	Ni foam	this work

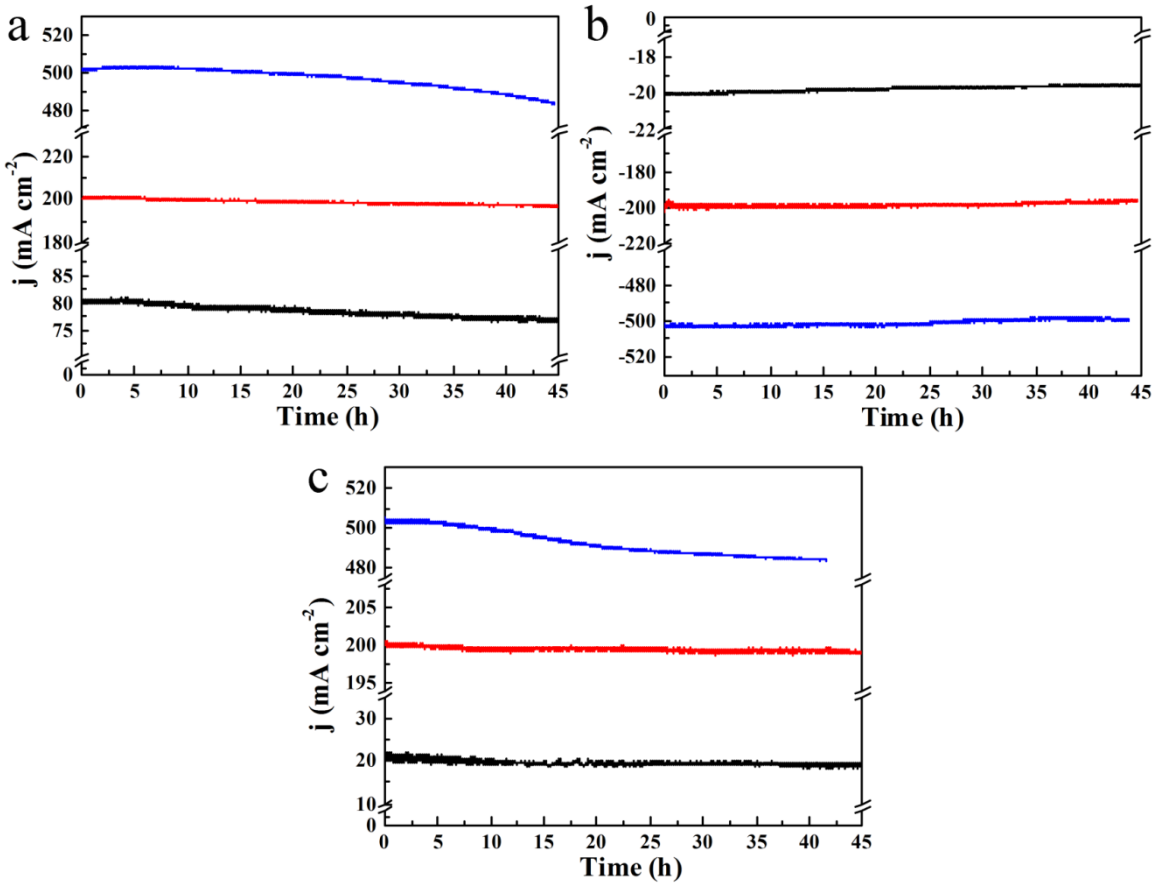

Figure S17. Chronoamperometric curves of $NiFe_2O_4$/NiFe LDH electrodes for exceeding 40 h for (a) OER at overpotentials of 202, 230 and 242 mV, respectively, (b) HER at overpotentials of 150, 259 and 298 mV, respectively, and (c) overall water splitting at a cell voltage of 1.60, 1.82 and 1.94 V, respectively.

REFERENCES

(1) Wu, Z.; Zou, Z.; Huang, J.; Gao, F. Fe-doped NiO Mesoporous Nanosheets Array for Highly Efficient Overall Water Splitting. *J. Catal.* **2018,** *358*, 243−252.

(2) Sun, Y.; Gao, S.; Lei, F.; Liu, J.; Liang, L.; Xie, Y. Atomically-Thin Non-Layered Cobalt Oxide Porous Sheets for Highly Efficient Oxygen-Evolving Electrocatalysts. *Chem. Sci.* **2014**, *5*, 3976−3982.

(3) Lu, X.; Zhao, C. Electrodeposition of Hierarchically Structured Three-dimensional Nickel-Iron

Electrodes for Efficient Oxygen Evolution at High Current Densities. *Nat. Commun.* **2015**, *6*, 6616.

(4) Liu, X.; Wang, X.; Yuan, X.; Dong, W.; Huang, F. Rational Composition and Structural Design of In Situ Grown Nickel-Based Electrocatalysts for Efficient Water Electrolysis. *J. Mater. Chem. A* **2016**, *4*, 167−172.

(5) Zou, X.; Liu, Y.; Li, G. D.; Wu, Y.; Liu, D. P.; Li, W.; Li, H. W.; Wang, D.; Zhang, Y.; Zou, X. Ultrafast Formation of Amorphous Bimetallic Hydroxide Films on 3D Conductive Sulfide Nanoarrays for Large-Current-Density Oxygen Evolution Electrocatalysis. *Adv. Mater.* **2017**, *29*, 1700404.

(6) Wang, J.; Ji, L.; Chen, Z. In Situ Rapid Formation of a Nickel–Iron-Based Electrocatalyst for Water Oxidation. *ACS Catal.* **2016**, *6*, 6987−6992.

(7) Song, F.; Hu, X. Exfoliation of Layered Double Hydroxides for Enhanced Oxygen Evolution Catalysis. *Nat. Commun.* **2014**, *5*, 4477.

(8) Li, Z.; Shao, M.; An, H.; Wang, Z.; Xu, S.; Wei, M.; Evans, D. G.; Duan, X. Fast Electrosynthesis of Fe-Containing Layered Double Hydroxide Arrays toward Highly Efficient Electrocatalytic Oxidation Reactions. *Chem. Sci.* **2015**, *6*, 6624−6631.

(9) Long, X.; Li, J.; Xiao, S.; Yan, K.; Wang, Z.; Chen, H.; Yang, S. A Strongly Coupled Graphene and FeNi Double Hydroxide Hybrid as an Excellent Electrocatalyst for the Oxygen Evolution Reaction. *Angew. Chem. Int. Ed.* **2014**, *53*, 7584−7588.

(10) Gao, Y. Q.; Liu, X. Y.; Yang, G. W. Amorphous Mixed-Metal Hydroxide Nanostructures for Advanced Water Oxidation Catalysts. *Nanoscale* **2016**, *8*, 5015−5023.

(11) Wang, H.-F.; Tang, C.; Zhang, Q. Towards Superior Oxygen Evolution through Graphene Barriers Between Metal Substrates and Hydroxide Catalysts. *J. Mater. Chem. A* **2015**, *3*,

16183−16189.

(12) Sun, X.; Shao, Q.; Pi, Y.; Guo, J.; Huang, X. A General Approach to Synthesise Ultrathin NiM (M = Fe, Co, Mn) Hydroxide Nanosheets as High-Performance Low-Cost Electrocatalysts for Overall Water Splitting. *J. Mater. Chem. A* **2017**, *5*, 7769−7775.

(13) Andronescu, C.; Barwe, S.; Ventosa, E.; Masa, J.; Vasile, E.; Konkena, B.; Moller, S.; Schuhmann, W. Powder Catalyst Fixation for Post-Electrolysis Structural Characterization of NiFe Layered Double Hydroxide Based Oxygen Evolution Reaction Electrocatalysts. *Angew. Chem. Int. Ed.* **2017**, *56*, 11258−11262.

(14) Bau, J. A.; Luber, E. J.; Buriak, J. M. Oxygen Evolution Catalyzed by Nickel-Iron Oxide Nanocrystals with a Nonequilibrium Phase. *ACS Appl. Mater. Interfaces* **2015**, *7*, 19755−19763.

(15) Wang, L.; Geng, J.; Wang, W.; Yuan, C.; Kuai, L.; Geng, B. Facile Synthesis of Fe/Ni Bimetallic Oxide Solid-Solution Nanoparticles with Superior Electrocatalytic Activity for Oxygen Evolution Reaction. *Nano Res.* **2015**, *8*, 3815−3822.

(16) Liu, G.; Gao, X.; Wang, K.; He, D.; Li, J. Mesoporous Nickel–Iron Binary Oxide Nanorods for Efficient Electrocatalytic Water Oxidation. *Nano Res.* **2017**, *10*, 2096−2105.

(17) Read, C. G.; Callejas, J. F.; Holder, C. F.; Schaak, R. E. General Strategy for the Synthesis of Transition Metal Phosphide Films for Electrocatalytic Hydrogen and Oxygen Evolution. *ACS Appl. Mater. Interfaces* **2016**, *8*, 12798−12803.

(18) Ganesan, P.; Sivanantham, A.; Shanmugam, S. Inexpensive Electrochemical Synthesis of Nickel Iron Sulphides on Nickel Foam: Super Active and Ultra-Durable Electrocatalysts for Alkaline Electrolyte Membrane Water Electrolysis. *J. Mater. Chem. A* **2016**, *4*, 16394−16402.

(19) Yan, J.; Wu, H.; Li, P.; Chen, H.; Jiang, R.; Liu, S. Fe(III) Doped NiS_2 Nanosheet: A Highly

Efficient and Low-Cost Hydrogen Evolution Catalyst. *J. Mater. Chem. A* **2017**, *5*, 10173−10181.

(20) Wang, P.; Pu, Z.; Li, Y.; Wu, L.; Tu, Z.; Jiang, M.; Kou, Z.; Amiinu, I. S.; Mu, S. Iron-Doped Nickel Phosphide Nanosheet Arrays: An Efficient Bifunctional Electrocatalyst for Water Splitting. *ACS Appl. Mater. Interfaces* **2017**, *9*, 26001−26007.

(21) Xiao, C.; Zhang, B.; Li, D. Partial-sacrificial-template Synthesis of Fe/Ni Phosphides on Ni Foam: a Strongly Stabilized and Efficient Catalyst for Electrochemical Water Splitting. *Electrochim. Acta* **2017**, *242*, 260−267.

(22) Wen, Z.; Li, H.; Ci, S.; Zhang, M.; Chen, J.; Lai, K. Facile Spray-Pyrolysis Synthesis of Yolk-Shell Earth-Abundant Elemental Nickel-Iron-Based Nanohybrid Electrocatalysts for Full Water Splitting. *ChemSusChem* **2017**, *10*, 4756−4763.

(23) Wu, S.; Shen, X.; Zhu, G.; Zhou, H.; Ji, Z.; Ma, L.; Xu, K.; Yang, J.; Yuan, A. Metal Organic Framework Derived NiFe@N-Doped Graphene Microtube Composites for Hydrogen Evolution Catalyst. *Carbon* **2017**, *116*, 68−76.

(24) Zhang, Z.; Qin, Y.; Dou, M.; Ji, J.; Wang, F. One-Step Conversion from Ni/Fe Polyphthalocyanine to N-Doped Carbon Supported Ni-Fe Nanoparticles for Highly Efficient Water Splitting. *Nano Energy* **2016**, *30*, 426−433.

(25) Jia, Y.; Zhang, L.; Gao, G.; Chen, H.; Wang, B.; Zhou, J.; Soo, M. T.; Hong, M.; Yan, X.; Qian, G.; Zou, J.; Du, A.; Yao, X. A Heterostructure Coupling of Exfoliated Ni-Fe Hydroxide Nanosheet and Defective Graphene as a Bifunctional Electrocatalyst for Overall Water Splitting. *Adv. Mater.* **2017**, *29*, 1700017.

(26) Zhang, X.; Xu, H.; Li, X.; Li, Y.; Yang, T.; Liang, Y. Facile Synthesis of Nickel–Iron/Nanocarbon Hybrids as Advanced Electrocatalysts for Efficient Water Splitting. *ACS Catal.*

2016, *6*, 580−588.